

Jiulong methane reef: Microbial mediation of seep carbonates in the South China Sea

Xiqiu Han ^{a,b}, Erwin Suess ^{b,c,*}, Yongyang Huang ^d, Nengyou Wu ^d, Gerhard Bohrmann ^e,
Xin Su ^f, Anton Eisenhauer ^b, Gregor Rehder ^g, Yinxia Fang ^a

^a Key Laboratory of Submarine Geosciences & Second Institute of Oceanography, State Oceanic Administration, Hangzhou 310012, China

^b Leibniz-Institute for Marine Sciences, 24148 Kiel, Germany

^c German Marine Research Consortium, 10117 Berlin, Germany

^d Guangzhou Marine Geological Survey, Guangzhou 510075, China

^e Geowissenschaften, University of Bremen, 28334 Bremen, Germany

^f China University of Geosciences, Beijing 100083, China

^g Institut für Ostseeforschung Warnemünde, 18119 Rostock-Warnemünde, Germany

Received 16 March 2007; received in revised form 9 November 2007; accepted 15 November 2007

Abstract

Chemoherm carbonates, as well as numerous other types of methane seep carbonates, were discovered in 2004 along the passive margin of the northern South China Sea. Lithologically, the carbonates are micritic containing peloids, clasts and clam fragments. Some are highly brecciated with aragonite layers of varying thicknesses lining fractures and voids. Dissolution and replacement is common. Mineralogically, the carbonates are dominated by high magnesium calcites (HMC) and aragonite. Some HMCs with MgCO₃ contents of between 30–38 mol%—extreme-HMC, occur in association with minor amounts of dolomite. All of the carbonates are strongly depleted in $\delta^{13}\text{C}$, with a range from -35.7 to -57.5% PDB and enriched in $\delta^{18}\text{O}$ ($+4.0$ to $+5.3\%$ PDB). Abundant microbial rods and filaments were recognized within the carbonate matrix as well as aragonite cements, likely fossils of chemosynthetic microbes involved in carbonate formation. The microbial structures are intimately associated with mineral grains. Some carbonate mineral grains resemble microbes. The isotope characteristics, the fabrics, the microbial structure, and the mineralogies are diagnostic of carbonates derived from anaerobic oxidation of methane mediated by microbes. From the succession of HMCs, extreme-HMC, and dolomite in layered tubular carbonates, combined with the presence of microbial structure and diagenetic fabric, we suggest that extreme-HMC may eventually transform into dolomites. Our results add to the worldwide record of seep carbonates and establish for the first time the exact locations and seafloor morphology where such carbonates formed in the South China Sea. Characteristics of the complex fabric demonstrate how seep carbonates may be used as archives recording multiple fluid regimes, dissolution, and early transformation events.

© 2007 Elsevier B.V. All rights reserved.

Keywords: methane seep carbonates; anaerobic methane oxidation; microbes; high Mg-calcite; South China Sea

1. Introduction

Methane-derived carbonates associated with chemosynthetic biota are known from seeps at active and passive continental margins world wide, e.g., at Cascadia margin (Kulm et al., 1986; Bohrmann et al., 1998; Greinert et al., 2001), the Gulf of

Mexico (Aharon et al., 1992), the Black Sea (Thiel et al., 2001), the Middle America margin (Bohrmann et al., 2002; Han et al., 2004), and the eastern Aleutian margin (Suess et al., 1998). Their formation is now widely accepted to be the result of anaerobic oxidation of methane (AOM) mediated by consortia of sulfate-reducing *Bacteria* and *Archaea* (Hinrichs et al., 1999; Boetius et al., 2000; Orphan et al., 2001). The ancient rock record also provides evidence for a relationship between microbes and carbonates at methane-seep settings. Extensive reviews of Devonian to Recent seep carbonates and of the

* Corresponding author. Leibniz-Institute for Marine Sciences (IFM-GEOMAR), 24148 Kiel, Germany. Tel.: +49 431 6002232; fax: +49 431 6002928.

E-mail address: esuess@ifm-geomar.de (E. Suess).

development of methane seep-environments through time are provided by Campbell et al. (2002) and by Campbell (2006), respectively. Current studies emphasize biomarkers, genetics and morphological criteria to firmly establish the presence of microbes in recent and ancient methane seep settings (Shapiro, 2004; Chen et al., 2005; Reitner et al., 2005; Birgel et al., 2008, and many others).

In June 2004 during the joint Chinese–German RV SONNE Cruise 177, areas of methane seepage were discovered in the South China Sea with buildups of carbonate caps on several ridges (Suess, 2005; Han et al., 2005). Since 2004, additional methane-derived carbonates have either been dredged from other locations of the South China Sea or had previously been collected there attesting to basin-wide methane seepage (Chen et al., 2005; Lu et al., 2005; Chen et al., 2006). The specific sites are at upper to middle slope depths. Buildups occur at three ridge-crest segments collectively covering about 400 km². Hundreds of carbonate samples were retrieved by TV-guided grabs as well as broken, whole, and disarticulated shells of bivalves including *Calyptogena* sp., *Acharax* sp., *Conchocele* sp., and *Bathymodiolus* sp. These are known to be chemosynthetic organisms from other methane-seep settings (Campbell, 2006). Based on field observations and laboratory studies of these samples, we present (1) a detailed description of the morphology, petrology, mineralogy, and isotope composition of these seep carbonates; show (2) diverse microbial structures preserved around and embedded in the carbonate matrix, thus supporting the role of anoxic oxidation of methane

(AOM) in their formation; and provide (3) evidence for the role of extreme-HMCs as precursors of dolomite.

2. Geologic setting and occurrence of seep carbonates

The South China Sea is a Cenozoic, Atlantic-type marginal sea of the western Pacific, bordered to the north and west by passive continental margins and to the east by the eastward-dipping ancient subduction zone of the Manila Trench (Taylor and Hayes, 1980; Pautot et al., 1986). The area of investigation is located at the transition between the passive northern margin and the accretionary eastern margin off SW Taiwan Island (Fig. 1). Here the seafloor morphology is characterized by deeply incised, NW–SE trending canyons, several of which appear to be fault-controlled (Ding et al., 2004). Sediments along the northern slope are several 100 to 10 000 m thick and thin out rapidly towards the center of the South China Sea basin. ODP Leg 184, drilled to the southwest of the area, showed that the sedimentation rate has been high – from 370–870 m/Ma – and that turbidite interbeds are common (Shipboard Scientific Party, 2000). There are strong bottom-simulating reflectors (BSRs) indicating abundant production of subsurface methane and the presence of gas hydrates (Song et al., 2001) which were successfully drilled at 153–225 m below sea floor in May 2007 (Zhang et al., 2007).

Seepage of methane-rich fluids on passive margins is generally driven by compaction of rapidly accumulating sediments. Fluid pathways are often poorly defined but occur along faults

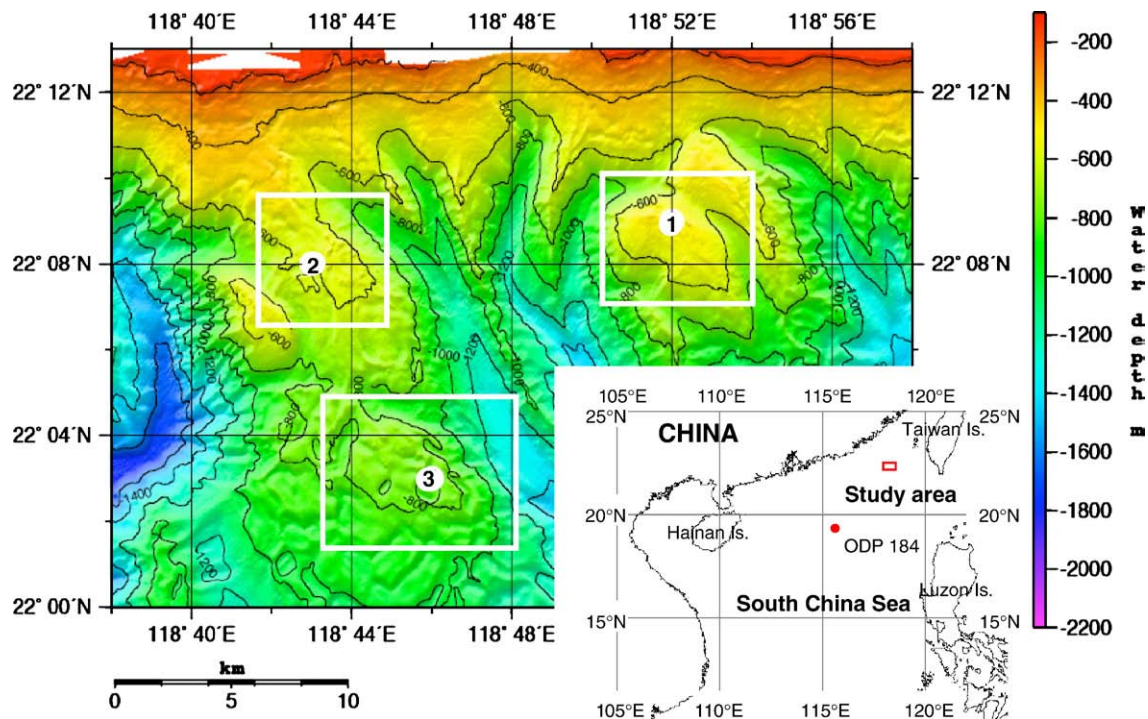


Fig. 1. Bathymetry of portion of the northern slope of the South China Sea showing areas of extensive seep carbonates at Sites 1, 2, and 3; sampling stations referred to in the text are for Site 1: TVG1, 2, and 3; for Site 2: TVG13 and 14; and for Site 3: TVG6, 8, 9, and 11, their positions are listed in Table 1. Inset: General location of study area.

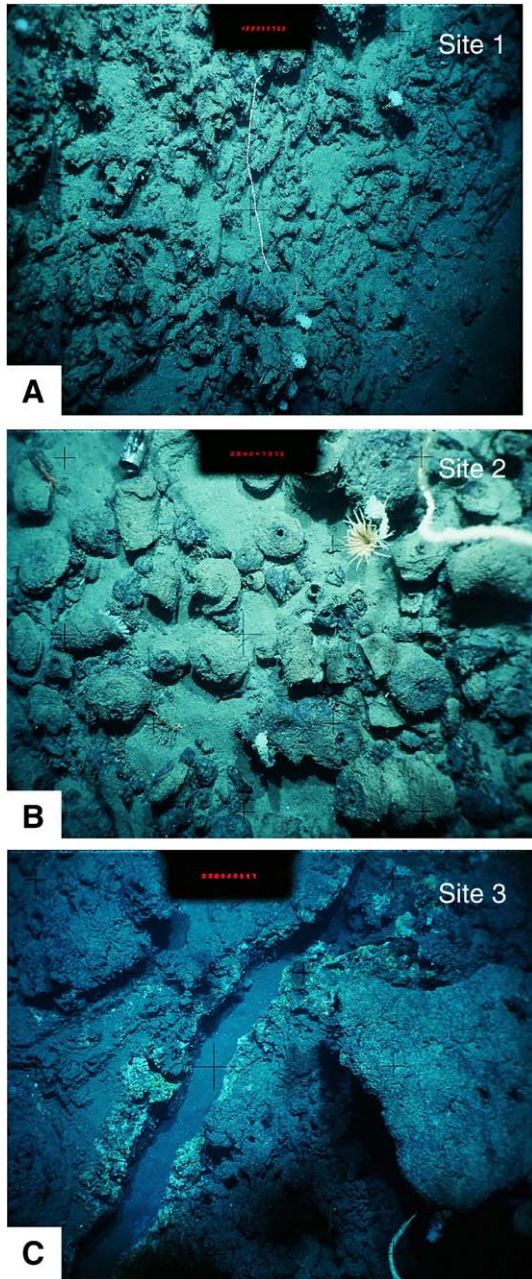


Fig. 2. Typical cold seep carbonates at the northern slope of the South China Sea. (A) Site 1: Field of carbonate rubble; tubular carbonates are several cms in diameter and up to 40 cm long. (B) Site 2: Protruding and broken carbonate chimneys; 4–10 cm in diameter. (C) Site 3: Chemoherm buildup; diameter of image approx. 150 cm; yellow and white bacterial patches lining wall fractures and rock surfaces.

developed through salt tectonics, differential compaction, or exposure of permeable strata through deformation. The South China Sea is underlain by oceanic basement dotted with volcanic structures. These structures are buried and several have developed deep-reaching faults along their flanks and upwards through the sediment column (Ding et al., 2004). It is conceivable that long-term fluid seepage, as well as development of chemoherm and methane-derived carbonates, occur at sites where such faults breach the seafloor.

Seep carbonates were sampled at three sites on two adjacent ridges. The majority of samples are comprised of blocks, concretions, slabs, crusts, chimney rubble, and cemented burrows and fluid channels. These are scattered at the seafloor or protrude from the sediment (Fig. 2A, B). At one site, Site 3, a carbonate edifice stands above the surrounding seafloor (Fig. 2C). It has been named Jiulong Methane Reef (Suess, 2005; Han et al., 2005). This site is still weakly active whereas the other sites are extinct.

2.1. Site 1

The shallowest site is located at 473–498 m depth. Investigation with an Ocean Floor Observation System (OFOS) showed that the seafloor is covered—in most places completely—by irregular doughnut-shaped, tabular and tubular carbonates and carbonate blocks (Fig. 2A). The rocks have a dark brown Fe–Mn coating, indicating that they have been exposed to the bottom water for some time. Three TV-guided grab samplers were deployed here and about 80 pieces of carbonates collected (TVG1, 2, 3; for positions see Table 1). The samples from TVG1 are dominated by tubular and doughnut-shaped concretions, 4–6 cm in diameter and 10–12 cm long. The orifice of central channels is about 2.5 cm in diameter; however, in some samples the central channels are completely filled in. They appear to be molds of burrows or fluid channels (Fig. 3A). An arrangement of circular holes in some samples (2–5 mm in diameter) contain thin, brown, chitinous wall residues that may have originated from tubeworms (Fig. 3B). Samples from TVG2 and TVG3 are dominated by blocks up to 100 cm across, tubular concretions, cemented burrows, and irregularly shaped concretions (Fig. 3C). The blocks are penetrated by borings and open flow structures with epibenthic organisms colonizing the surface. White aragonite layers are common, lining voids or filling the conduits of tubular concretions. It appears that this site was active in the past but now is inactive and subject to exhumation by strong bottom currents.

Table 1

Locations of seep carbonates from the northern slope of the South China Sea

Location	Latitude	Longitude	Depth (m)
<i>Site 1</i>			
TVG1	22° 09.06' N	118° 52.34' E	498
TVG2	22° 08.94' N	118° 52.37' E	484
TVG3	22° 08.96' N	118° 52.34' E	473
<i>Site 2</i>			
TVG13	22° 08.54' N	118° 43.45' E	555
TVG14	22° 08.63' N	118° 43.39' E	533
<i>Site 3</i>			
TVG6	22° 02.85' N	118° 46.58' E	769
TVG7	22° 02.83' N	118° 46.54' E	768
TVG8	22° 02.85' N	118° 46.55' E	769
TVG9	22° 02.85' N	118° 46.54' E	771
TVG11	22° 02.86' N	118° 46.51' E	769

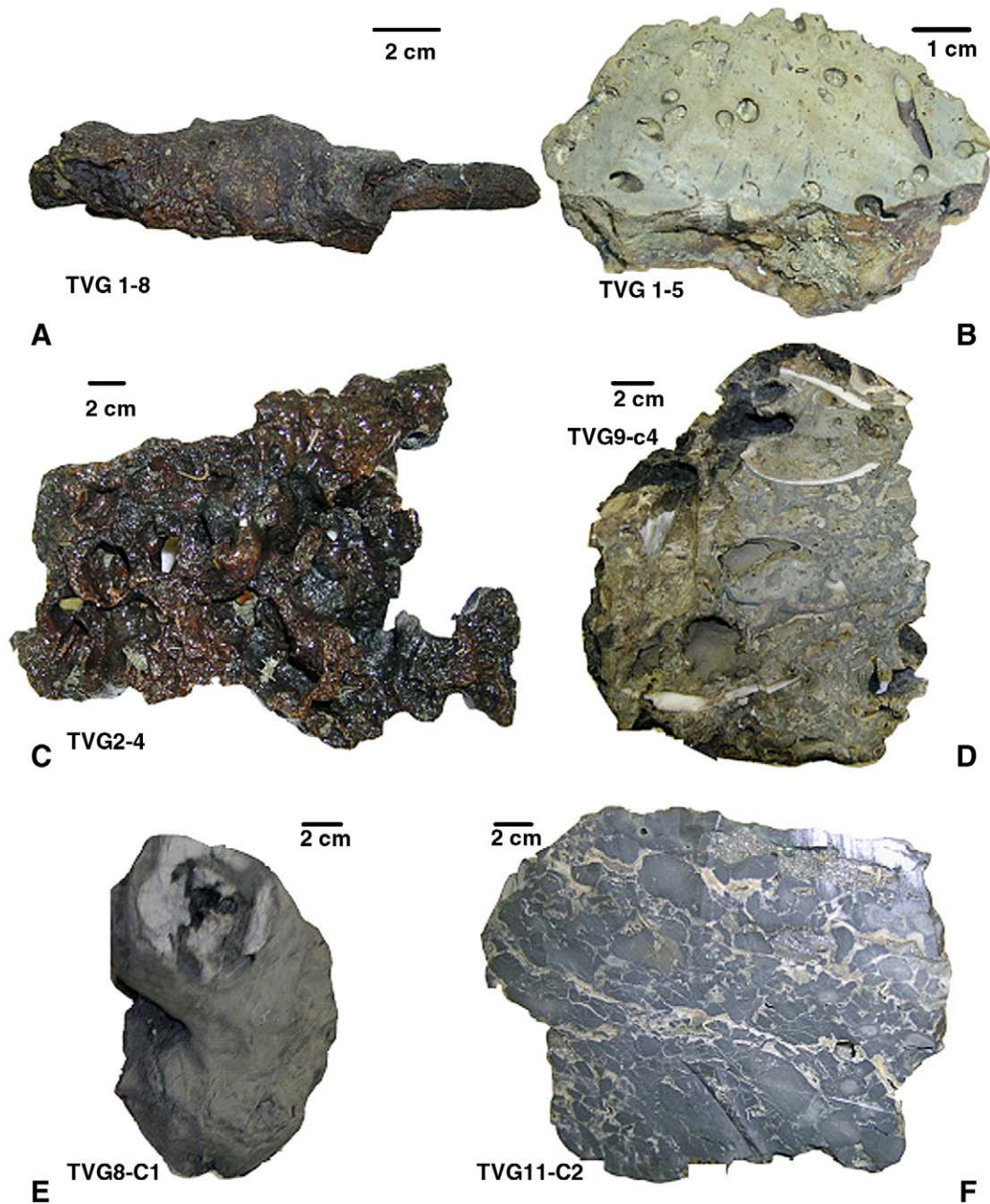


Fig. 3. Typical morphologies of seep carbonates. (A) Tubular concretions: Mold of bioturbation tube or fluid channel; Fe–Mn oxide coating; TVG1-8, Site 1. (B) Massive slab: Abundant mm-sized holes with chitinous walls probably originating from tube worms; TVG1-5, Site 1. (C) Irregular tabular concretion: Fe–Mn coating, interconnected circuitous channels and protuberances; TVG2-4, Site 1. (D) Chemoherm fragment: Abundant cemented shell debris; aragonite void linings; elongated layered voids (1–6×1–2 cm) with fresh sediment fill; TVG9-C4, Site 3. (E) Carbonate chimney: Fresh appearance; central orifice 2–4 cm diameter; soft clay filling; TVG8-C1, Site 3. (F) Carbonate breccia: Network of aragonite-filled fractures; matrix highly brecciated and cemented; TVG11-C2, Site 3.

2.2. Site 2

This site is located to the west of Site 1 at around 550 m water depth. A field of carbonate, chimneys, and rubble was discovered on the ridge crest (Fig. 1). Two TV-guided grabs (TVG13, 14; for positions see Table 1) yielded mostly carbonate chimneys 8–40 cm long and 4–10 cm in diameter and chimney fragments. Most have a brownish Fe–Mn coating; they protrude from sediments or lie broken on the seafloor (Fig. 2B). Some

tubular samples more slender than the chimneys are irregular in shape with numerous nodular protuberances and open fluid channels. These are likely cemented conduits formed at or below the sediment surface and were later winnowed out.

2.3. Site 3

This is the deepest site (762–768 m) and located at the southern end of the same ridge where Site 2 was found (Fig. 1).

OFOS images show the chemoherm buildup, Jiulong Methane Reef, about 30 m high, above a base at least 100 m in diameter (Fig. 2C). There are irregular yellowish and whitish bacterial patches on the surface of the chemoherm blocks, lining fractures as well as on the sediment surface (Fig. 2C). Slightly elevated methane concentrations in the bottom water (3 nmol/L; Suess, 2005) and the bacterial linings indicate that this site is still active. Five TVG-sampler deployments (TVG6, 7, 8, 9, 11; for positions see Table 1) retrieved mostly chemoherm blocks (Fig. 3D), rather fresh greenish–gray chimneys (Fig. 3E), as well as breccias cemented by aragonite (Fig. 3F). The variety of carbonate morphologies and types here was by far the greatest among the three sites.

3. Materials and methods

All of the rock specimens were first examined and described on board ship. Forty-six representative samples were then selected for shore-based petrological, mineralogical, and isotopic analyses. Subsamples of these were taken to represent different stages of carbonate formation, e.g., matrix vs. cement, inner vs. outer layer, wall vs. interior, yielding a total of 60 samples. Thin sections of representative samples were prepared for petrographic investigation using a Leica DMLP light microscope. The mineralogy of all carbonate samples was determined by X-ray diffraction (XRD) analyses using a Philips PW 1820 diffractometer. The XRD patterns were obtained from 3° to 70° 2-Theta at a low scan speed of 0.02° per second. The d [101] peak of quartz was used as internal standard. The mol-percentage of MgCO₃ in calcite was calculated from the d [104]-shift using the average of the linear correlation provided by Goldsmith et al. (1961) and Lumsden (1979). Calcite containing <5 mol% MgCO₃ is considered low-Mg calcite (LMC); otherwise, it is referred to as high-Mg calcite (HMC) with the mol% of MgCO₃ given. The relative weight percentages of HMC, LMC, aragonite, and minor dolomite were calculated using the linear correlation between XRD-intensity and quantity as given by Milliman (1977). Carbon- and O-isotope ratios were measured on a Finnigan MAT 252 mass spectrometer. CO₂ extraction for $\delta^{13}\text{C}$ and $\delta^{18}\text{O}$ measurements was carried out with pure H₃PO₄ at 75 °C. Replicate analyses of a laboratory standard show a standard deviation better than 0.03‰ for $\delta^{13}\text{C}$ and 0.01‰ for $\delta^{18}\text{O}$. All data are reported relative to the PDB standard. XRD-results and stable isotope compositions are listed in Table 2. Samples for Scanning Electron Microscopy (SEM) and Energy Dispersive X-ray spectroscopy (EDAX) analysis were prepared on freshly broken surfaces to avoid contamination. They were analyzed on Hitachi S-4700 II SEM, equipped with Thermo NORAN Vantage ESI EDS.

4. Results

4.1. Types of authigenic carbonate and morphology

The morphology, fabric, texture and stable isotope composition of all samples is consistent with chemoherm carbonates (Fig. 3D, F) and seepage-associated carbonates (Fig. 3A–C, E). Among the seepage-associated carbonates, chimneys (Fig. 3E),

tubular concretions (Fig. 3A), massive and tabular lithologies are differentiated (Fig. 3B, C). The criteria and the general lithotype descriptions are as follows.

4.1.1. Chemoherm carbonates

Chemoherm refers to buildup of precipitated chemical carbonates with calcareous skeletal debris of chemosynthetic fauna, having an anomalously negative carbon isotope composition (Aharon, 1994). The free standing edifice-type configuration is important because it signifies sustained focused seepage of methane-rich fluids exiting into the free bottom water (Teichert et al., 2005).

Typical chemoherm carbonate blocks were sampled at Jiulong Methane Reef, Site 3. Fig. 3D shows a fragment from a larger block such as shown in Fig. 2C. It contains abundant shell debris, and the surface is rough with many protuberances (~0.5 cm in diameter). The size of the cemented shell is up to 1 cm thick and 9 cm long. The pore spaces are completely or partially filled by aragonite and sediments. Fig. 3F shows a highly brecciated block with elongated layered voids (1–6 × 1–2 cm). A network of aragonite layers as thick as 8 mm lines most of these voids. Besides chemoherm blocks much chemoherm debris was collected at Jiulong Methane Reef. Some of it appeared fresh and weakly cemented, dark gray with mottled greenish–blue portions, other pieces seemed more worn with a yellowish surface.

4.1.2. Seepage-associated carbonates

This type occurs on the seafloor or the subsurface. It differs from chemoherms in forming carbonate slabs, concretions, crusts, and tubes. Tubular carbonates and chimneys were retrieved as well as tabular and massive carbonates. The chimneys are 4–20 cm long, 3.5–5 cm in diameter with a central fluid conduit (Fig. 3E); however, some were completely or partially filled by one or more generations of aragonite or HMC. The tubular carbonates are smaller and more slender than the chimneys (1.5–3.5 cm in diameter), and typically, without a central channel, they appear to be either cemented burrows or fluid conduits (Fig. 3A). Tabular and massive carbonates now blanket the seafloor but appear to have formed in the subsurface and subsequently been winnowed out. They exhibit unusual shapes, difficult to classify by morphology alone. The numerous thin and circuitous channels suggest formation associated with slow fluid flow regimes (Fig. 3C).

4.2. Petrology of authigenic carbonates and diversity of microbial structures

The carbonate lithologies vary between micrite, pelmicrite, thrombolite and biomicrite. Only chemoherm carbonates contain all four, whereas seepage-associated carbonates lack biomicrite. The micrite is mainly composed of microcrystalline HMC with minor silt-sized quartz and plagioclase. The pelmicrites contain 15–80% peloids (size: 0.6–1.8 mm) and acicular aragonite is often seen radiating from peloids (Fig. 4A). Thrombolite is found in the aragonite filling of tubular carbonates as well as the aragonite layer of chemoherm carbonates. It contains clots with abundant dark organic matter and

Table 2
Mineralogy, stable isotopes, and mineral percentages of the carbonate fraction of samples from the South China Sea; those in italics are imaged in Fig. 3

Sample code	Description and sampling position	$\delta^{13}\text{C}$ (PDB‰)	$\delta^{18}\text{O}$ (PDB‰)	Relative weight percentage (%)						
				LMC	HMC with MgCO_3 (mol%)				Dolo.	Arag.
					5–10	10–15	15–20	30–40		
TVG1-1	Massive	-49.90	3.82	0	0	100	0	0	0	0
TVG1-6	Massive	-48.97	3.73	0	0	100	0	0	0	0
TVG1-7A	Chimney, outer layer	-40.33	1.71	0	100	0	0	0	0	0
TVG1-7B	Chimney, inner layer	-52.14	2.92	0	0	100	0	0	0	0
<i>TVG1-8A</i>	Tubular, outer layer	-52.51	3.52	0	0	100	0	0	0	0
<i>TVG1-8B</i>	Tubular, core	-50.95	3.42	0	0	100	0	0	0	0
TVG1-13	Tubular	-50.50	3.96	7	0	93	0	0	0	0
TVG1-16	Massive	-54.77	3.09	5	0	32	0	0	1	62
TVG2-1A	Tubular, outer layer	-55.62	3.38	0	0	0	50	0	0	50
TVG2-1C	Tubular, filling	-56.16	3.12	5	0	0	0	0	0	95
TVG2-1B	Tubular, core	-46.75	3.43	0	0	0	0	0	0	100
TVG2-2	Chimney	-54.30	3.63	9	0	0	64	7	1	19
TVG2-3A	Chimney, outer layer	-42.70	2.86	12	0	0	83	3	0	1
TVG2-3B	Chimney, filling	-52.05	3.48	0	0	41	0	0	0	59
TVG2-3C	Chimney, core	-42.52	3.28	3	0	86	0	0	0	12
<i>TVG2-4</i>	Tabular	-44.22	3.77	0	24	0	69	7	0	0
TVG3-3A	Massive, matrix	-48.88	3.42	0	0	46	0	0	0	54
TVG3-3B	Massive, cement	-35.70	3.27	1	0	0	0	0	0	99
TVG6-8-2	Tubular	-55.58	4.79	5	0	0	95	0	0	0
TVG6-9-2	Massive	-52.27	4.58	4	0	0	89	6	1	0
TVG7-15-1	Chemoherm	-52.02	4.31	1	0	20	0	0	0	79
TVG7-16	Chemoherm	-51.34	4.84	11	0	76	0	0	0	13
TVG8-C8-1	Massive	-52.86	4.78	0	0	94	0	0	0	6
TVG8-C5-2A	Tubular, outer layer	-51.29	4.80	0	0	100	0	0	0	0
TVG8-C5-2B	Tubular, core	-48.28	5.28	6	0	42	0	52	0	0
TVG8-C5-3	Tubular	-49.13	4.29	5	0	63	0	0	2	30
TVG8-C6-2	Tabular	-50.59	4.57	11	0	80	0	9	1	0
TVG8-C8-1-1	Tubular	-47.05	4.44	6	0	0	82	0	1	12
TVG8-C2-1	Massive	-54.24	4.72	18	0	0	51	30	1	0
TVG-9-C1-1A	Chemoherm, cement	-49.46	4.16	3	0	0	0	0	0	97
TVG-9-C1-1B	Chemoherm, matrix	-48.07	3.93	10	0	17	0	0	0	73
<i>TVG9-C4A</i>	Chemoherm, outer layer	-52.59	3.88	15	0	0	0	0	0	85
<i>TVG9-C4B</i>	Chemoherm, cement	-51.64	4.11	9	0	18	0	0	0	73
<i>TVG9-C4C</i>	Chemoherm, filling	-50.37	4.02	6	0	3	0	0	0	91
TVG11-C2-1A	Chemoherm, cement	-56.71	4.06	5	0	0	0	0	0	95
TVG11-C2-1B	Chemoherm, matrix	-51.32	4.80	5	0	63	0	19	2	11
TVG11-C1-4-1A	Tubular, filling	-55.48	4.80	17	0	0	54	29	0	0
TVG11-C1-4-1B	Tubular, wall	-54.91	4.44	11	0	55	0	24	0	10
TVG11-C1-2	Massive	-55.75	4.88	10	0	70	0	19	1	1
<i>TVG11-C2-5A</i>	Chemoherm, cement	-52.67	4.14	3	0	0	0	0	0	97
TVG11-C2-5A-1	Aragonite, outer layer	-57.55	3.90	0	0	13	0	0	0	87
TVG11-C2-5B-2	Aragonite, inner layer	-56.46	4.03	0	0	13	0	0	0	87
TVG11-C2-5B	Chemoherm, matrix	-51.23	5.16	0	0	69	0	30	2	0
TVG13-C1-1A	Chimney, outer layer	-45.97	2.93	0	84	0	0	12	4	0
TVG13-C1-1B	Chimney, 2nd layer	-48.55	3.44	0	84	0	0	14	1	0
TVG13-C1-1C	Chimney, 3rd layer	-48.88	3.35	0	0	92	0	8	0	0
TVG13-C1-1D	Chimney, inner layer	-42.60	1.96	7	0	90	0	0	3	0
TVG13-C1-2	Chimney	-43.63	2.75	0	94	0	0	3	3	0
TVG13-C1-3	Chimney	-45.68	3.20	0	99	0	0	0	1	0
TVG13-C1-5	Chimney	-43.79	3.35	0	90	0	0	7	2	0
TVG13-C4-1	Chimney	-41.15	2.29	45	0	40	0	12	4	0
TVG13-C5-1	Tabular	-45.31	3.64	16	0	0	53	28	3	0
TVG14-C1-1A	Chimney, outer layer	-47.54	3.11	15	0	42	0	41	1	0
TVG14-C1-1B	Chimney, middle layer	-46.83	3.25	15	0	49	0	36	1	0
TVG14-C1-1C	Chimney, inner layer	-50.47	3.99	26	0	0	0	72	2	0
TVG14-C2-1	Tubular	-49.88	4.08	8	0	0	68	22	2	0
TVG14-C2-2	Tubular	-47.84	4.21	4	0	0	81	14	1	0
TVG14-C2-3A	Tubular, filling	-56.33	3.71	0	0	0	99	0	1	0
TVG14-C2-3B	Tubular, outer layer	-54.36	3.44	0	0	0	99	0	1	0
TVG14-C2-4	Tubular	-50.02	4.00	9	0	0	83	8	0	0

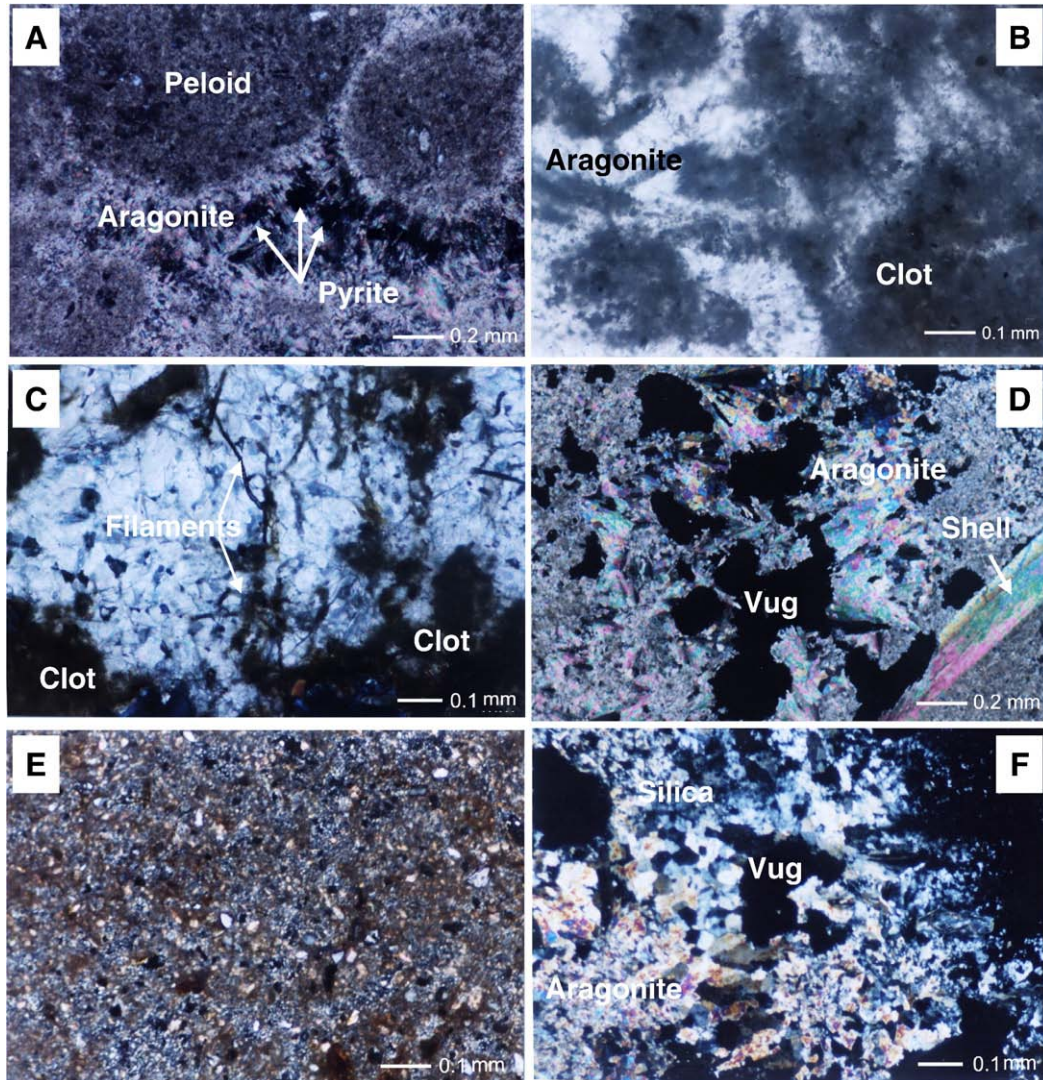


Fig. 4. Photomicrographs of typical fabric of authigenic carbonates. (A) Aragonite cemented peloids: Framboidal pyrite among aragonite; chemoherm carbonate TVG11-C2-1; cross-polarized light. (B) Thrombolitic fabric: Aragonite cemented; clots are rich in organic matter with indistinct boundaries, aragonite cement filling pore space; tubular concretion TVG2-1; plane-polarized light. (C) Microbial filaments: Embedded in aragonite; filaments are 0.1–0.6 mm long, 0.01 mm diameter, hollow and segmented; tubular concretion TVG2-1; cross-polarized light. (D) Dissolution features: Aragonite cement and clam shell are locally dissolved; carbonate chimney TVG9-C4; cross-polarized light. (E) Extensive silification, very fine-grained chalcedony replaced the host HMC; doughnut-shaped concretion TVG13-C1-2. Cross-polarized light. (F) Authigenic silica precipitated after aragonite in pore space; chemoherm carbonate TVG9-C4; cross-polarized light.

indistinct margins (Fig. 4B). Occasionally, segmented microbial filaments (0.1–0.6 mm long, 0.01 mm diameter) were observed in aragonites associated with clots or peloids (Fig. 4C). Biomicrites contain abundant bioclasts (e.g., whole and fragmented shells of *Bivalves*, *Gastropods*, and *Foraminifera*), peloids, clots and clasts (Fig. 4D). Layers of botryoidal aragonite line the voids and fractures. Authigenic framboidal pyrite (0.5–0.7 mm diameter) is present both in the matrix and the aragonite cements of all samples (Fig. 4A); this indicates formation in the sulfate reduction zone.

Dissolution is common, as are partially dissolved clam shells (Fig. 4D). Silification is observed in a micritic carbonate chimney progressing from the wall inward with a silica content of as much as 50 vol.% (Fig. 4E). In some voids of biomicrite from chemoherm carbonates, the aragonite lining is partly replaced by silica (Fig. 4F).

The sequence of carbonate formation and dissolution is different for samples from different sites and hence their paragenetic events are not identical. An idealized sequence, based on our observations, may have been as follows: (i) Early stage of cementation by microcrystalline HMC and/or aragonite as primary cement, with occasional framboidal pyrite forming; (ii) Dissolution stage creating pinholes in micrite; (iii) Neomorphic spar replacement in magnesium calcite precipitated around pinholes; (iv) Intermediate stage of cementation by fibrous aragonite radiating from peloids and precipitated in pores and micro fractures; (v) Corrosion and dissolution creating voids, micro fractures and irregular surfaces of peloids and detrital grains which were lined in places with pyrites or iron (hydroxy)-oxides; (vi) Latest stage of carbonate cementation by pervasive botryoidal aragonite formed in voids; (vii) Renewed partial dissolution of aragonite void linings;

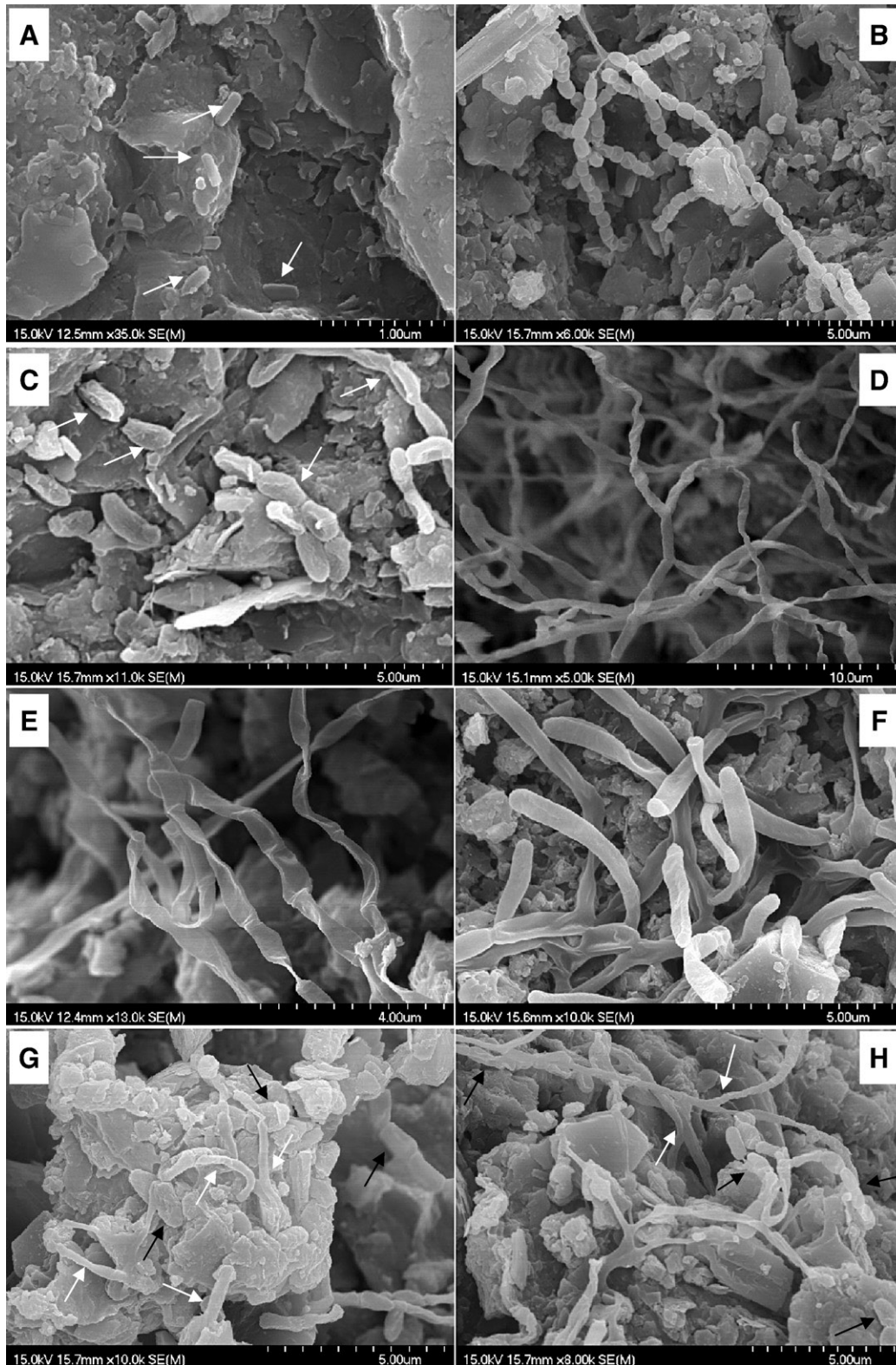


Fig. 5. Diversity of microbial structures preserved in authigenic carbonates, SEM micrographs. (A) Rod-shaped microbes with square ends (white arrows); $0.06\text{--}0.1\ \mu\text{m}$ in diameter, $0.15\text{--}0.3\ \mu\text{m}$ in length, biofilms also present; sample TVG 3-3. (B) Rod-shaped microbes with rounded ends; size: $0.6\text{--}0.8\ \mu\text{m}$ in diameter and $0.8\text{--}1.2\ \mu\text{m}$ in length; tend to form long chains; sample TVG11-C2-1. (C) Same as image B, showing disjointed chains (white arrows), some rods appear wrinkled; size: $0.5\text{--}0.8\ \mu\text{m}$ wide, $0.8\text{--}1.4\ \mu\text{m}$ long; sample TVG 11-C2-1. (D) Filamentous microbes forming mat; sample TVG7-16-1. (E) Enlargement of previous image D; filaments are flat, segmented and twisted; each segment is about $0.4\text{--}0.7\ \mu\text{m}$ in diameter and $1.1\text{--}2.5\ \mu\text{m}$ in length, new filament sprout at the joint of segments; sample TVG13-C1-1. (F) Similar to image E; filaments are less flattened; sample TVG14-C2-3. (G) Cylindrical filamentous microbes (white arrows); diameters $0.2\text{--}0.5\ \mu\text{m}$; co-occur with rod-shaped microbes (black arrows); $7\ \mu\text{m}$ in diameter; sample TVG11-C2-1. (H) Cylindrical filaments of considerable length, $10\text{--}20\ \mu\text{m}$ (white arrows); black arrows point to rod-shaped chains of microbes as in image G; sample TVG 11-C2-1.

Table 3
Characteristics of preserved microbes and their frequency in seep carbonates

Type	Description	Diameter (μm)	Length (μm)	Frequency (%)
1	Rod-shaped microbes with square ends	0.06–0.1	0.15–0.3	12
2	Rod-shaped microbes with rounded ends; tending to form chains	0.5–0.8	Rods: 0.6–1.8 Chains: 6–20	25
3	Flat filaments, segmented and spiraled; new segments sprouting from joints	0.5–0.8	Filaments: 10 s Segments: 1–2.5	54
4	Cylinder-shaped filaments; grow together with Type 2, sometimes forming aggregates	0.2–0.4	Aggregates in diameter: 2–10	9

(viii) Partial replacement of HMC and aragonite around the pores of voids by silica and fine-grained quartz.

Abundant microbial structures were observed under SEM (Fig. 5). According to their sizes and morphologies, the following types were differentiated and summarized in Table 3: (1) Rod-shaped microbes with square ends, between 0.06–0.1 μm in diameter and 0.15–0.3 μm in length (Fig. 5A; in sample TVG3-3 from Site 1). (2) Rod-shaped microbes with rounded ends, between 0.5 and 0.8 μm in diameter and 1.3 to 2.5 μm in length. The rods remain joined at nodes, forming strings of microbes (Fig. 5B). Sometimes the strings are disjointed with the individual rods appearing wrinkled, probably due to dehydration (Fig. 5C; commonly observed in samples from Sites 2 and 3). (3) Flat filaments that are segmented and twisted. Each segment is about 0.4–0.7 μm wide and 1–2.5 μm long. New filaments appear to have sprouted from joints of segments; the filaments tended to form mats (Fig. 5D, E, F). This type is common in samples from chemoherm carbonates (Sample TVG7-16), bioturbation tubes (Sample TVG14-C2-3), and chimneys (Sample TVG13-C1-1). (4) Cylinder-shaped filaments between 0.2–0.4 μm in diameter and 2–4 μm in length (Fig. 5G). They often appear together with rod-shaped microbes with rounded ends, and as aggregates of about 7 μm in diameter (Fig. 5G). Sometimes these filaments are elongated, forming microbial chains as long as 20 μm (Fig. 5H).

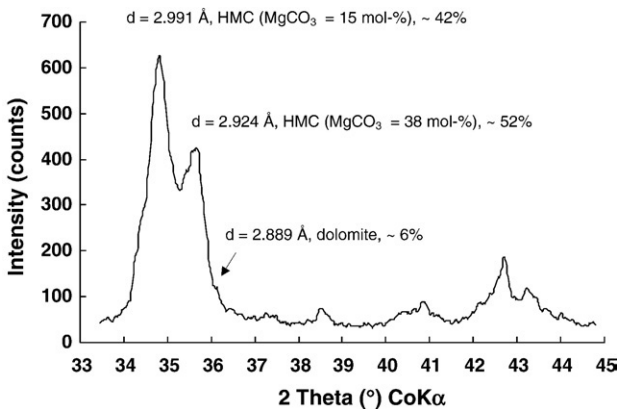


Fig. 6. XRD-pattern of two Mg-calcite phases, one having 15 mol% MgCO_3 and the other 38 mol% MgCO_3 ; minor amount of dolomite present; mineral weight percentages are approximately: 42 wt.%, 52 wt.%, and 6 wt.%; sample TVG8-C5-2B.

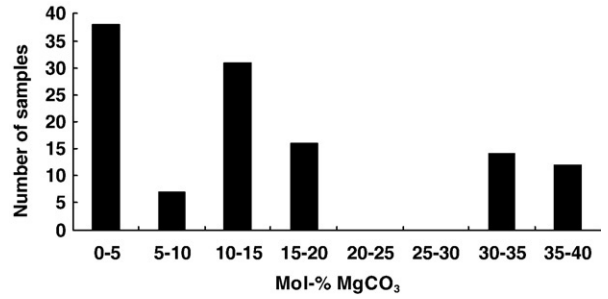


Fig. 7. Frequency distribution of HMC of all carbonate samples analyzed from the South China Sea sites. Most contain HMC with MgCO_3 content <20 mol%; some contain extreme-HMCs with magnesium contents of up to 38 mol% MgCO_3 .

4.3. Mineralogy of carbonates and the role of extreme-HMC

X-ray diffraction analysis shows that the carbonates are dominated by HMC and aragonite with minor amounts of LMC and dolomite (Table 2). Minor quartz, feldspar, clays and traces of pyrite were also identified. A few samples contained a small amount of gypsum. The mineral compositions are similar to samples from the Costa Rica margin (Han et al., 2004) and are typical for seep carbonates world wide (Campbell, 2006). There is a unique HMC-phase, however, with MgCO_3 of up to 38 mol% present among the South China Sea carbonates. These unusual HMCs are referred to as extreme-HMCs. Fig. 6 shows a typical XRD pattern of such extreme-HMCs: two calcite peaks at d [104]-spacing of 2.9908 Å and 2.9240 Å, indicating that there are two HMC phases present, one with 15 mol% and the other with 38 mol% MgCO_3 . Besides HMCs, there is a small amount of dolomite present. The relative mineral weight percents are 42% for HMC, 52% for extreme-HMC, and 6% for dolomite (Fig. 6). All of the three sites contain extreme-HMCs and small amounts of dolomite. The number of samples with different amounts of MgCO_3 -substitution in calcite is shown in Fig. 7.

For any sample with multiple magnesian calcites, older layers appear to contain more and better-crystallized extreme-HMC than younger layers. This is best illustrated in sample TVG13-C1-1 (Fig. 8). The inner part of the carbonate chimney is composed of HMC with 12 mol% MgCO_3 , a small amount of extreme-HMC as indicated by the broad peak on the shoulder, and no detectable dolomite. The middle layer shows the dominant HMC-peak as before, a strong extreme-HMC-peak with 34 mol% MgCO_3 , plus a detectable amount of dolomite. In the outer layer there is still a dominant HMC-peak, a yet stronger extreme-HMC peak with 35 mol% MgCO_3 , as well as a clear dolomite peak. Since the inner layer of the chimney formed later than the outer, this sequence indicates that more and better-crystallized extreme-HMC developed over time, eventually resulting in transformation to dolomite. This succession is unlike that observed in carbonate crusts formed in contact with bottom water.

4.4. C- and O-isotope compositions

The stable C- and O-isotope composition of all carbonate samples is listed in Table 2 and illustrated in Fig. 9. As expected,

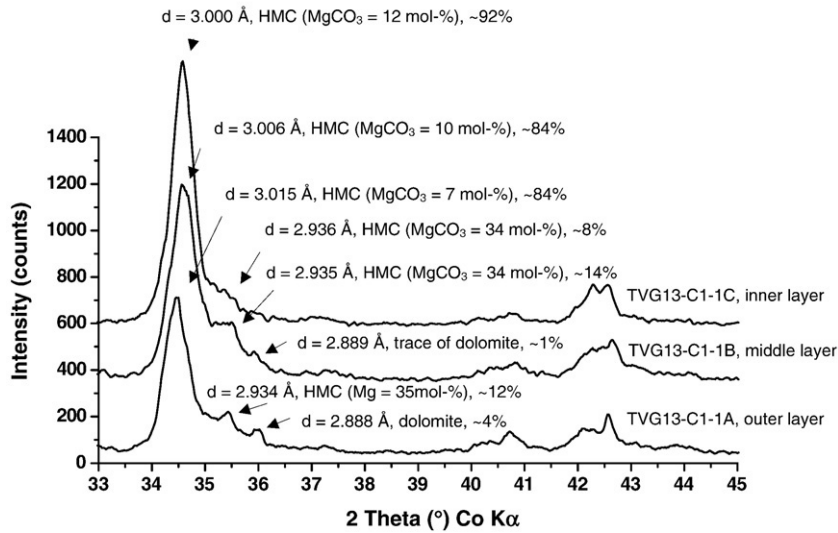


Fig. 8. XRD-patterns of three successive layers of the same carbonate chimney; trends of more extreme-HMCs and presence of dolomite occur from the inner layer (younger) to the outer layer (older), suggesting early diagenetic transformation; sample TVG13-C1-1.

they differ significantly from other marine carbonates in their strongly depleted $\delta^{13}\text{C}$ -values and slightly enriched $\delta^{18}\text{O}$ -values. In this respect they are very similar to isotope characteristics of seep carbonates reported elsewhere and summarized by Campbell (2006). The data confirm that the samples formed as a result of microbiological anaerobic oxidation of methane (AOM) where mostly biogenic methane is supplied as a fluid component from below the seafloor. While there is no significant systematic difference in the C-isotope values among the 3 sites, it is worth noting that heavier C-isotopes are derived from samples at shallower sites (Sites 1 and 2) and lighter C-isotopes largely from the deeper Site 3. The opposite trend is observed in the O-isotope data. These observations are summarized in Table 4. As a first approximation, the trend in O-isotopes is taken as a temperature

effect on the carbonate formation due to the highly stratified water column. As for the C-isotope trend, where the fractionation between aragonite and calcite would need to be considered, later generations usually have more depleted $\delta^{13}\text{C}$ than earlier ones. For example, the matrix has heavier C-isotopes than the cement. An exception is sample TVG3-3B, which is a seepage-associated carbonate crust. Its matrix has a C-isotope value of -48.9‰ PDB; however, its later aragonite cement has the heaviest C-isotope value of all the samples (-35.7‰ PDB). Besides biogenic methane there is probably some thermogenic methane involved here.

5. Discussion

5.1. Evidence for the involvement of microbes in the formation of seep carbonates

Microbial mats consisting of sulfate-reducing, sulfide-oxidizing and methane-oxidizing microbes are present at active seep sites (Sassen et al., 1993; Hinrichs et al., 1999; Boetius et al., 2000; Reitner et al., 2005). Using Fluorescent In Situ Hybridization techniques (FISH), it has been demonstrated that consortia of sulfate-reducing bacteria and archaeal species are responsible for the oxidation of methane and the formation of seep carbonates (Hinrichs et al., 1999; Boetius et al., 2000; Orphan et al., 2001). The C-isotopes, in the range of -35.7 to

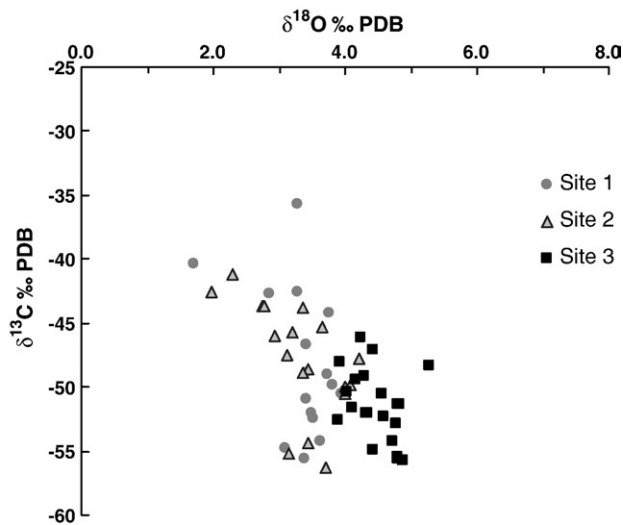


Fig. 9. Carbon- and O-isotope composition of all seep carbonates analyzed from the South China Sea grouped according to sites; trend in $\delta^{18}\text{O}$ reflects changes in temperature of water column; trend in $\delta^{13}\text{C}$ appears related to different methane sources.

Table 4

Ranges of stable isotope composition of seep carbonates; change in $\delta^{18}\text{O}$ with water depths appears to reflect change in temperature of bottom water; change in $\delta^{13}\text{C}$ appears to reflect different methane sources

Location	Water depth (m)	$\delta^{13}\text{C}$ (‰ PDB)		$\delta^{18}\text{O}$ (‰ PDB)	
		Range	Average	Range	Average
Site 1	473 to 498	-35.7 to -55.6 ($n=18$)	-48.8	1.7 to 4.0	3.3
Site 2	533 to 555	-41.1 to -56.3 ($n=18$)	-47.6	2.0 to 4.2	3.3
Site 3	762 to 768	-48.1 to -56.7 ($n=34$)	-51.9	3.9 to 5.3	4.5

–57.5 PDB‰, indicate unequivally that the South China Sea carbonates are derived from AOM mediated by microbes.

Our SEM-images show that there are abundant microbial structures preserved in the carbonates. Among them, the flat and spiraled filaments with segments may represent sulfide oxidizers (Fig. 5D, E, F) described as *Beggiatoa*-like by Peckmann et al. (2004) and by Barbieri and Cavalazzi (2005). The rod-shaped microbes with rounded ends (Fig. 5B, C, G, H) bear some similarity to *Archaea*, both in size and morphology, as observed in methane-rich sediments, bacterial mats, and concretionary carbonates from the Black Sea (Pimenov et al., 1997; Michaelis et al., 2002; Reitner et al., 2005). The cylinder-shaped filaments (Fig. 5G) are similar to sulfate-reducing bac-

teria (SRB) isolated from Lagoa Vermelha samples (van Lith et al., 2003). Interestingly, the two types of microbes often grow together to form aggregates that resemble SRB and *Archaea* consortia as shown by Boetius et al. (2000).

The morphology of some mineral grains strongly resemble microbes. In sample TVG3-3, where rod-shaped microbes with square ends are present (Fig. 5A), numerous rod-shaped aragonite grains (0.06–0.2 μm wide, 0.2–0.8 μm long; Fig. 10A) are observed as well. These grains are likely the fossilized rod-shaped bacterial bodies. EDAX-analysis showed that some of the microbial filaments (Fig. 10C) are composed of HMC. Also TVG2-1 contains traces of dolomite, and many spindle- and half dumbbell-shaped nano-grains (0.2–0.7 μm wide, 0.7–1.7 μm

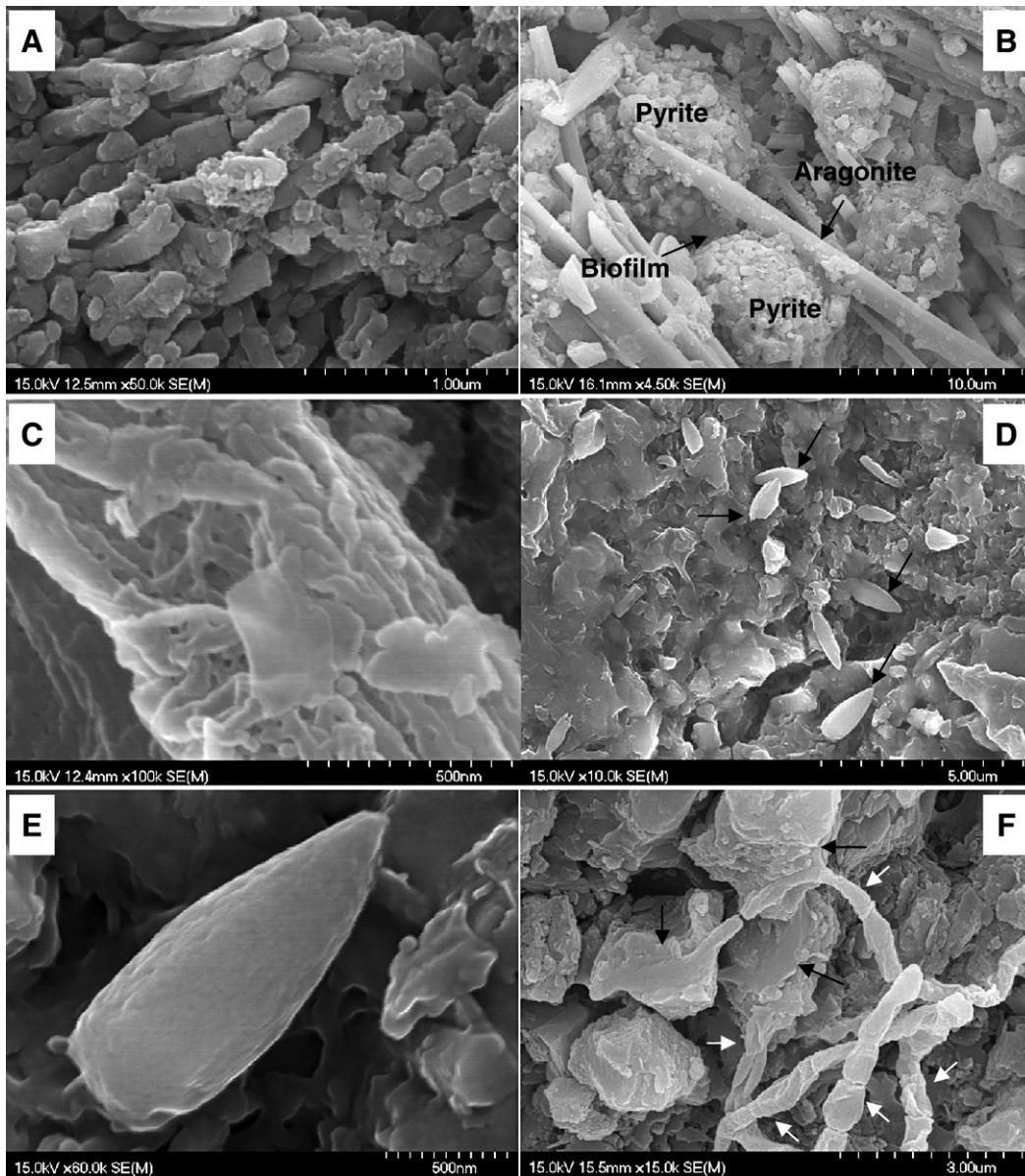


Fig. 10. Relationships of microbial structures and carbonate minerals; SEM micrographs; scales are at bottom of each image. (A) Aragonite grains: Same morphology and size of rod-shaped microbes as shown in Fig. 5A; size 0.06–0.2 μm wide, 0.2–0.8 long; sample TVG 3-3. (B) Pyrite framboids (4–9 μm in diameter): With aragonite needles (1–2 μm wide, 10–30 μm long) in the presence of biofilm indicating that both may have formed in the sulfate reduction zone; sample TVG11-C2-1. (C) Filaments: Microbial structures consisting of HMC based on EDAX pattern (not shown); sample TVG14-C2-3. (D) Spindle-shaped grains: Assumed to be dolomite and associated with biofilm; size 0.5–1 μm ; sample TVG2-1. (E) Enlargement of previous image. (F) Filaments: Apparently fossilized and associated with cauliflower-shaped extreme-HMC or dolomite; sample TVG14-C2-3.

long; Fig. 10D, E) are present. The grains strongly resemble morphologies of biogenic dolomite precipitated in a simulated sedimentary environment using SRBs cultured from Lagoa Vermelha samples (Vasconcelos and McKenzie, 1997; van Lith et al., 2003). Fig. 10F shows a cauliflower-shaped mineral grain formed at the end of a rod-shaped microbial chain. This configuration is very similar to that of dolomite and microbes shown by Warthmann et al. (2000). These associations are important evidence for fossilized microbes embedded in the carbonates rather than modern contamination. Although the preserved microbes described here are not conclusively identified, all of the above evidence demonstrates that they are intimately related to the formation of the carbonate minerals. Most recently, a set of newly recognized biomarkers (biphytanic diacids) in seep limestones, that are almost exclusively derived from methanotropic *Euryarchaea*, were isolated from the chemoherm sample TVG11-C2-5 (Birgel et al., 2008). They are highly ^{13}C -depleted ($\delta^{13}\text{C} = -132$ PDB‰) and occur in concert with other biomarkers characteristic of AOM.

5.2. Extreme-HMC and implication for dolomite formation

XRD-analysis showed that some carbonate samples contain multiple HMC-phases with Mg-contents ranging from 5–20 mol% and from 30–38 mol% (Fig. 7). HMCs commonly contain $\text{MgCO}_3 < 20\%$ whereas extreme-HMCs are rarely reported in the literature. To our knowledge extreme-HMCs have only been reported once previously and that is from carbonates at hydrocarbon seeps of the Gulf of Mexico (Ferrell and Aharon, 1994). Vasconcelos and McKenzie (1997) identified two HMC phases corresponding to 12 and 35 mol% MgCO_3 along with LMC and dolomite in black sludge samples from Lagoa Vermelha, however the HMC formation mechanism and any relationship with dolomite remained unclear. Ferrell and Aharon (1994) also reported an almost identical frequency distribution of mol% Mg-calcites as shown in Fig. 8 with the characteristic miscibility gap between 20–30 mol%. The authors consider these phases to be Ca-rich dolomites based on progressive XRD-peak width and mol% MgCO_3 and corresponding prominent dolomite peaks. They were unable to further characterize the calcian dolomites, however, because of insufficient amount available in the complex mineral mixtures of the Gulf of Mexico samples. Our samples clearly contain traces of dolomite concurrent with major HMC-percentages (Fig. 6) suggesting the presence of two separate phases, HMC and dolomite, rather than a single calcian dolomite.

The South China Sea samples may provide further insight into the formation of dolomite by transformation of extreme-HMCs as gleaned from sample TVG13-C1-1A to C (Table 2 and Fig. 8). The inner layer, being the youngest and freshest precipitate, contains in its carbonate mineral fraction 92 wt.% of 10–15 mol% HMC, 8 wt.% of extreme-HMC, and no dolomite. The outer layer, being the oldest precipitate and having undergone diagenesis, contains 84 wt.% of 5–10 mol% HMC, 12 wt.% of extreme-HMC and 4 wt.% dolomite. The middle layer shows transitional characteristics.

Crystallinity is better developed in the outer layer than in the inner (Fig. 8) also suggesting a time-dependent formation of

dolomite at the expense of HMCs and extreme-HMCs. Partial dissolution, cementation, and replacement are common in those samples containing extreme-HMC and dolomite (Fig. 4E). Isotopes are slightly enriched in $\delta^{13}\text{C}$ and more depleted in $\delta^{18}\text{O}$ for the outer layers, not just in sample TVG13-C1-1 but in others with similarly discernable layering as well (TVG1-7; TVG2-3; TVG11-C1-4; TVG14-C1-1; TVG14C2-3). These differences range from 0.6 to 10.4 PDB‰ for $\delta^{13}\text{C}$, and from –0.3 to –0.9 PDB‰ for $\delta^{18}\text{O}$. We think that they are partly caused by alteration through seawater.

Based on observations in a hypersaline and anoxic dolomite-precipitating lagoon (Lagoa Vermelha, Brazil), Vasconcelos and McKenzie (1997) proposed a microbial dolomite model. This model suggested that the activity of sulfate-reducing bacteria plays an active role in dolomite precipitation. It remains unresolved, however, whether or not the dolomites were transformed from HMC with the participation of bacteria. From our observations and those of Ferrell and Aharon (1994), we emphasize that transformation is a mechanism in eventually forming dolomite from moderately high primary-HMC and extreme-HMC.

6. Conclusions

Two types of seep carbonates, chemoherm and seepage-associated carbonates, were discovered at the South China Sea sites. Chemoherm are large buildups, 10s of meters in elevation above the surrounding seafloor that grow upward into the bottom-water driven by continuous and vigorous flow of methane-rich fluids. Chemoherm carbonates are mostly aragonitic. Seepage-associated carbonates form on or just below the seafloor at less vigorous seepage rates. They develop many different shapes and sizes, with chimneys and burrow-fillings quite common. The crusts are composed predominantly of high magnesium calcites (HMC), minor aragonite, and minor dolomite. Among these phases are extreme-HMCs with MgCO_3 of up to 38 mol%. From the succession and composition of HMCs, extreme-HMCs and dolomite in well-defined, layered carbonates, we suggest that transformation is an important process in the eventual formation of seep dolomites.

Abundant microbial rods and filaments, presumably representing archaeal species and SRBs involved in AOM, were documented. Although not conclusively identified, the abundant evidence shows that microbes are intimately associated with the formation of carbonate minerals, as would be expected in AOM-generated seep carbonates. Their role in determining the mineralogy is intriguing but currently not sufficiently clear.

Acknowledgments

We thank the R/V SONNE 177 crew and shipboard scientific parties for their cooperation and highly professional help at sea. We thank Bettina Domeyer for help with sample preparation, Ralf Tiedemann (IFM-GEOMAR, Kiel) for C- and O- isotope analyses, Jutta Heinze (IFM-GEOMAR, Kiel) for assistance with XRD analysis, Yifan Zhen (Zhejiang University of Technology) for assistance with SEM and Zona Sues for help with the

English. We also thank two anonymous reviewers whose many comments greatly helped to focus the topic of the paper. This study was funded by the German Ministry of Science and Education (BMBF Az 03G0177A) and financial support for ship-time by the Geological Survey of China (GCS) through the Guangzhou Marine Geological Survey (GMGS). The work of X. Han was supported through the National Science Foundation of China (NSFC No. 40476050), GMGS-grant and the Chinese Ministry of Personnel grant. Additional support to E. Suess was provided through GMGS-grant D0990. This study is part of the Chinese-German cooperation project (SiGer) through the GEOTECHNOLOGY initiative, contribution number GEOTECH-285.

References

- Aharon, P., 1994. Geology and biology of modern and ancient submarine hydrocarbon seeps and vents: an introduction. *Geo Mar. Lett.* 14, 69–73.
- Aharon, P., Roberts, H.H., Snelling, R., 1992. Submarine venting of brines in the deep Gulf of Mexico: observations and geochemistry. *Geology* 20, 483–486.
- Barbieri, R., Cavalazzi, B., 2005. Microbial fabrics from Neogene cold seep carbonates, Northern Apennine, Italy. *Palaeogeogr. Palaeoclimatol. Palaeoecol.* 227, 143–155.
- Birgel, D., Elvert, M., Han, X., Peckmann, J., 2008. ^{13}C -depleted biphytanic diacids as tracers of past anaerobic oxidation of methane. *Org. Geochem.* 39, 152–156.
- Boetius, A., Ravensschlag, K., Schubert, C.J., Rickert, D., Widdel, F., Gieseke, A., Amann, R., Jørgensen, B.B., Witte, U., Pfannkuche, O., 2000. A marine consortium apparently mediating anaerobic oxidation of methane. *Nature* 407, 623–626.
- Bohrmann, G., Greinert, J., Suess, E., Torres, M., 1998. Authigenic carbonates from the Cascadia subduction zone and their relation to gas hydrate stability. *Geology* 26 (7), 647–650.
- Bohrmann, G., Heeschen, K., Jung, C., Weinrebe, W., Baranov, B., Cailleau, B., Heath, R., Huehnerbach, V., Hort, M., Mason, D., 2002. Widespread fluid expulsion along the seafloor of the Costa Rica convergent margin. *Terra Nova* 14 (2), 69–79.
- Campbell, K.A., 2006. Hydrocarbon seep and hydrothermal vent palaeoenvironments: past developments and future research directions. *Palaeogeogr. Palaeoclimatol. Palaeoecol.* 232, 362–407.
- Campbell, K.A., Farmer, J.D., Des Merays, D., 2002. Ancient hydrocarbon seeps from the Mesozoic convergent margin of California: carbonate geochemistry, fluids and paleoenvironments. *Geofluids* 2, 63–94.
- Chen, D.F., Huang, Y.Y., Yuan, X.L., Cathles III, L.M., 2005. Seep carbonates and preserved methane oxidizing bacteria and sulfur reducing bacteria fossils suggest recent gas venting on the seafloor in the northeastern South China Sea. *Mar. Pet. Geol.* 22, 613–621.
- Chen, Z., Yan, W., Chen, M., Wang, S., Lu, J., Zhen, F., Xiang, R., Xiao, S., Yan, P., Gu, S., 2006. Discovery of seep carbonate nodules as new evidence for gas venting on the northern continental slope of South China Sea. *Chin. Sci. Bull.* 51 (10), 1228–1237.
- Ding, W., Wang, Y., Chen, H., Yang, S., Wu, N., 2004. Deformation characters and its tectonic evolution of the Southwest Taiwan Basin. *J. of Zhejiang Univ. (Science Edition)*, vol. 31(2), pp. 216–220 (Chinese with English abstract).
- Ferrell Jr., R.E., Aharon, P., 1994. Mineral assemblages occurring around hydrocarbon vents in the Gulf of Mexico. *Geo Mar. Lett.* 14, 74–80.
- Goldsmith, J.R., Graf, D.L., Heard, H.C., 1961. Lattice constants of the calcium-magnesium carbonates. *Am. Mineral.* 46, 453–457.
- Greinert, J., Bohrmann, G., Suess, E., 2001. Gas hydrate-associated carbonates and methane-venting at Hydrate Ridge: classification, distribution and origin of authigenic lithologies. In: Paull, C.K., Dillon, W.P. (Eds.), *Natural Gas Hydrates: Occurrence, Distribution and Detection*. Geophys. Monogr. American Geophysical Union, Washington, DC, pp. 99–113.
- Han, X., Suess, E., Sahling, H., Wallmann, K., 2004. Fluid venting activity on the Costa Rica margin: new results from authigenic carbonates. *Int. J. Earth Sci. (Geol Rundschau)* 93, 596–611.
- Han, X., Suess, E., Huang, Y., Wu, N., Eisenhauer, A., Bohrmann, G., Su, X., Rehder, G., Fang, Y., shipboard scientists of Leg SO-177, 2005. Jiulong Methane reef: first direct evidence of methane seepage in the South China Sea. *Geophysical Research Abstracts* 7, 04055. European Geosciences Union.
- Hinrichs, K.-U., Hayes, J.M., Sylva, S.P., Brewer, P.G., Delong, E.F., 1999. Methane-consuming archaeobacteria in marine sediments. *Nature* 398, 802–805.
- Kulm, L.D., Suess, E., Moore, J.C., Carson, B., Lewis, B.T., Ritger, S.D., Kadko, D.C., Thornburg, T.M., Embley, R.W., Rugh, W.D., Massoth, G.J., Langseth, M.G., Cochrane, G.R., Scamman, R.L., 1986. Oregon subduction zone: venting, fauna, and carbonates. *Science* 231, 561–566.
- Lu, H., Liu, J., Chen, F., Liao, Z., Sun, X., Su, X., 2005. Mineralogy and stable isotope composition of authigenic carbonates in bottom sediments on the offshore area of southwest Taiwan, South China Sea: evidence for gas hydrates occurrence. *Earth Sci. Frontiers* 12, 268–276 (in Chinese with English abstract).
- Lumsden, D.S., 1979. Discrepancy between thin-section and X-ray estimates of dolomite in limestone. *J. Sediment. Petrol.* 49, 429–436.
- Michaelis, W., Seifert, R., Nauhaus, K., Treude, T., Thiel, V., Blumenberg, M., Knittel, K., Gieseke, A., Peterknecht, K., Pape, T., Boetius, A., Amann, R., Jørgensen, B.B., Widdel, F., Peckmann, J., Pimenov, N.V., Gulin, M.B., 2002. Microbial reefs in the Black Sea fueled by anaerobic oxidation of methane. *Science* 297, 1013–1015.
- Milliman, J., 1977. Role of calcareous algae in Atlantic continental margin sedimentation. In: Fluegel, E. (Ed.), *Fossil Algae*. Springer, Berlin, pp. 232–247.
- Orphan, V.J., House, C.H., Hinrichs, K.-U., McKeegan, K.D., DeLong, E.F., 2001. Methane-consuming Archaea revealed by directly coupled isotopic and phylogenetic analysis. *Science* 293, 484–487.
- Pautot, G., Rangin, C., Briais, A., Tapponier, P., Beuzart, P., Lericolais, G., Mathieux, X., Wu, Y., Han, S., Li, Y., Zhao, J., 1986. Spreading direction in the central South China Sea. *Nature* 321, 150–154.
- Peckmann, J., Thiel, V., Reitner, J., Taviani, M., Aharon, P., Michaelis, W., 2004. A microbial mat of a large sulfur bacterium preserved in a Miocene methane-seep limestone. *Geomicrobiol. J.* 21, 247–255.
- Pimenov, N.V., Rusanov, I.I., Poglazova, M.N., Mityushina, L.L., Sorokin, D.Y., Khmelena, V.N., Trotsenko, Y.A., 1997. Bacterial mats on coral-like structures at methane seeps in the Black Sea. *Microbiology* 66, 354–360 (translated from *Mikrobiologiya*).
- Reitner, J., Peckmann, J., Blumenberg, M., Michaelis, W., Reimer, A., Thiel, V., 2005. Concretionary methane-seep carbonates and associated microbial communities in Black Sea sediments. *Palaeogeogr. Palaeoclimatol. Palaeoecol.* 223, 18–30.
- Sassen, R., Roberts, H.H., Aharon, P., Larkin, J., Chinn, E.W., Carney, R., 1993. Chemosynthetic bacterial mats at cold hydrocarbon seeps, Gulf of Mexico continental slope. *Org. Geochem.* 20, 77–89.
- Shapiro, R.S., 2004. Recognition of fossil prokaryotes in Cretaceous methane seep carbonates: relevance to astrobiology. *Astrobiology* 4 (4), 438–449.
- Shipboard Scientific Party, 2000. Leg 184 Summary: Exploring the Asian Monsoon Through Drilling in the South China Sea. In: Wang, P., Prell, W.L., Blum, P. (Eds.), *Proc. ODP, Init. Repts.*, vol. 184. Ocean Drilling Program, College Station TX, pp. 1–77.
- Song, H.-B., Geng, J.-H., Wong, H.K., Zhang, W.-S., Fang, Y.-X., Hao, T.-Y., Jiang, W.-W., 2001. A preliminary study of gas hydrates in the Dongsha region, northern South China Sea. *Chin. J. Geophys.* 44 (5), 684–691.
- Suess, E., 2005. RV SONNE cruise report SO 177. Sino-German cooperative project, South China Sea Continental Margin: geological methane budget and environmental effects of methane emissions and gas hydrates. IFM-GEOMAR Reports. <http://store.pangaea.de/documentation/Reports/SO177.pdf>.
- Suess, E., Bohrmann, G., von Huene, R., Linke, P., Wallmann, K., Lammers, S., Sahling, H., Winckler, G., Lutz, R.A., Orange, D., 1998. Fluid venting in the eastern Aleutian subduction zone. *J. Geophys. Res.* 103, 2597–2614.
- Taylor, B., Hayes, D.E., 1980. The tectonic evolution of the South China Basin. In: Hayes, D.E. (Ed.), *Tectonic and Geologic Evolution of Southeast Asian Seas and Islands*. Geophys. Monogr., vol. 23. American Geophysical Union, pp. 89–104.
- Teichert, B.M.A., Bohrmann, G., Suess, E., 2005. Chemohermes on hydrate ridge — unique microbially-mediated carbonate buildups growing into the water column. *Palaeogeogr. Palaeoclimatol. Palaeoecol.* 227 (1–3), 67–85.

- Thiel, V., Peckmann, J., Richnow, H.H., Luth, U., Reitner, J., Michaelis, W., 2001. Molecular signals for anaerobic methane oxidation in Black Sea seep carbonates and a microbial mat. *Mar. Chem.* 73, 97–112.
- van Lith, Y., Warthmann, R., Vasconcelos, C., McKenzie, J.A., 2003. Microbial fossilization in carbonate sediments: a result of the bacterial surface involvement in dolomite formation. *Sediment* 50, 237–245.
- Vasconcelos, C., McKenzie, J.A., 1997. Microbial mediation of modern dolomite precipitation and diagenesis under anoxic conditions (Lagoa Vermelha, Rio de Janeiro, Brazil). *J. Sediment. Res.* 67, 378–390.
- Warthmann, R., van Lith, Y., Vasconcelos, C., McKenzie, J.A., Karpoff, A.-M., 2000. Bacterially induced dolomite precipitation in anoxic culture experiments. *Geology* 28 (12), 1091–1094.
- Zhang, H., Yang, S., Wu, N., Schultheiss, P., GMGS-1 science team, 2007. China's first gas hydrate expedition successful. *Fire in the Ice: Methane Hydrate Newsletter*, National Energy Technology Laboratory, U.S Department of Energy, Spring/Summer issue, 1.